Laser induced micro-cracking of Zr-based metallic glass using 10^{11} W/m^2 nano-pulses

Hu Huang[a,*], Yongfeng Qian[a], Chao Wang[a], Jiwang Yan[b,*]

[a] Key Laboratory of CNC Equipment Reliability, Ministry of Education, School of Mechanical and Aerospace Engineering, Jilin University, Changchun, Jilin, 130022, China
[b] Department of Mechanical Engineering, Faculty of Science and Technology, Keio University, Yokohama 223-8522, Japan

A B S T R A C T

Low power nanosecond laser irradiation has potential applications in surface processing of metallic glasses (MGs). However, the response of MGs to a relatively low power intensity (10^{11} W/m^2) has not been investigated. In this study, surface microstructures and characteristics of Zr-based MG after low power nanosecond laser irradiation were studied. Micro-cracks with depth in nanoscale and width in microscale were observed on the irradiated MG surface. The effects of laser parameters on the formation and evolution of micro-cracks were further investigated, and surface characteristics were characterized by using X-ray diffraction (XRD) and energy dispersive X-ray spectroscopy (EDS). The results showed that under the peak laser power intensity of 2.3×10^{11} W/m^2, when increasing the scanning speed from 1 to 5 mm/s, the maximum width of micro-cracks reduced from 3 μm to be less than 1 μm; further increasing to 10 mm/s, no micro-cracks appeared. When increasing the laser power intensity, the micro-groove structure would be formed with pileup around it and line cracks, open cracks and laser pulse tracks on it. During multi-line laser scanning, the pulse overlap rate also affected the formation and distribution of micro-cracks. At last, the formation mechanism of micro-cracks was discussed. These results would be meaningful for understanding the laser-MG interaction as well as guiding the selection of laser parameters for various applications.

1. Introduction

In recent years, metallic glasses (MGs) as a kind of emerging materials have become the focus of research due to their excellent mechanical, physical, and chemical properties, such as high strength and hardness, excellent anti-corrosion, and anti-wear features [1–4]. These unique properties make MGs become very promising materials for applications in the fields of defense and aerospace, sport products, consumer electronics, and so on [5]. However, currently, the practical applications of MGs, especially as the structural materials, still face some problems such as the very low tensile plasticity, difficulty in machining by conventional mechanical methods due to the inherent hard-brittle nature of MGs, and limitation in dimension due to the requirement of fast cooling rate during the preparation process. To solve these problems, a lot of technologies have been introduced or newly proposed in the field of MGs in the past years. Among them, laser technology as a versatile tool has been also employed to process MGs [6], providing some alternative methods for solving the aforementioned problems. For example, by laser welding and additive manufacturing, the size of MGs could be effectively enlarged [7–11]; by laser shock

peening, mechanical properties of MGs could be tuned [12–15]; by laser machining or laser patterning, micro/nano-structures could be fabricated on the surface of MGs, enhancing their functional applications [16–21].

During the above studies, both the continuous laser and pulsed laser have been used. As MGs are sensitive to temperature, the pulsed laser is better for avoiding the crystallization. Taking advantages of relatively short pulse duration, low cost and high efficiency, nanosecond pulsed laser has been widely employed to process MGs [19,20,22]. For example, via nanosecond pulsed laser shock peening, residual compressive stress could be introduced into the MGs, being beneficial to improving the plasticity of MGs [23]. Via nanosecond pulsed laser patterning, various microstructures such as ripples [24], Saffman-Taylor fingering [25], porous structure [26], and hierarchical micro/nano-structures [16,17], have been formed on the surface of MGs, which could enhance their applications as functional materials. By nanosecond pulsed laser irradiation in nitrogen gas, Zr-based MG could be nitrided, and its surface hardness and microscale plastic deformation behaviors could be tuned [27]. To realize laser surface modification or laser patterning of MGs, a relatively high peak laser power intensity
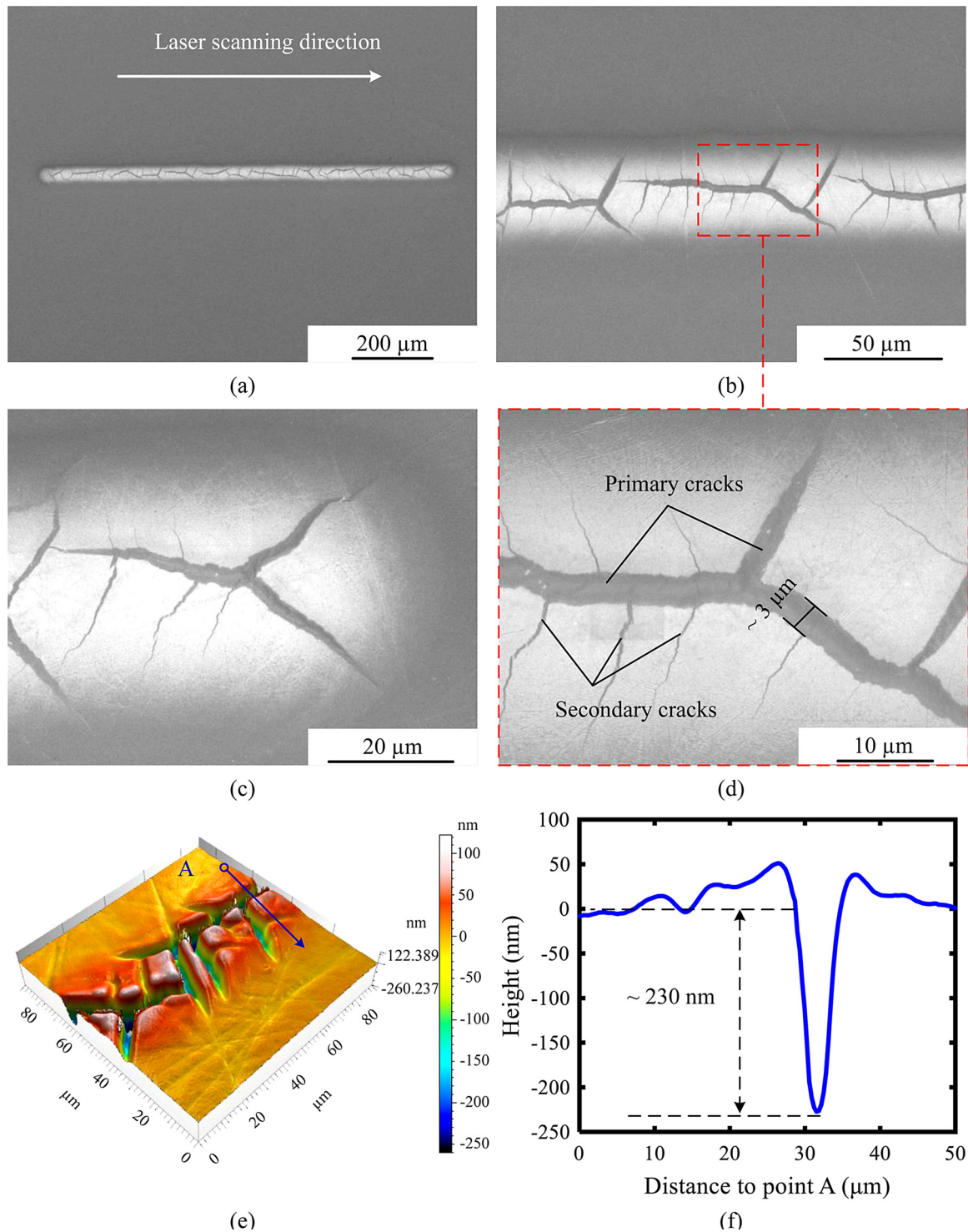
---

* Corresponding authors.
  E-mail addresses: huanghu@jlu.edu.cn (H. Huang), yan@mech.keio.ac.jp (J. Yan).

Fig. 1. (a) SEM morphology of the MG surface after single-line scanning under a peak laser power intensity of 2.3×10^{11} W/m^2 and scanning speed of 1 mm/s, (b) local enlarged SEM image around the center of the scanning line, (c) local enlarged SEM image around the end of the scanning line, (d) local enlarged SEM image showing the primary crack and secondary crack in detail. (e) 3D topography of the irradiated region and (f) the profile of the marked line in Fig. 1(e).

being greater than 10^{12} W/m^2 was commonly employed, and correspondingly, the MG surface would been severely ablated [17,20,24,26]. Therefore, the current understanding of nanosecond laser-MG interaction is obtained under the relatively high laser power intensity; while, the response of MGs to a relatively low laser power intensity (for example 10^{11} W/m^2) has not been investigated. In addition, high power nanosecond laser processing such as laser shock peening and laser additive manufacturing generally results in poor surface quality of MGs,

which restricts the practical applications of processed MGs. As laser irradiation with a low power intensity has potential applications in surface polishing/planarization of laser shock peened and additively manufactured MGs, it is meaningful to investigate the surface characteristics of MGs after low power nanosecond laser irradiation.

Accordingly, in this study, a Zr-based MG surface was irradiated by using a nanosecond pulsed laser with relatively low laser power intensity (10^{11} W/m^2), being an order of magnitude lower than the

commonly used one. The results showed that micro-cracks with depth in nanoscale and width in microscale were induced on the MG surface. By changing the experimental parameters, the effects of laser power intensity and scanning speed on the surface characteristics were comparatively investigated. After that, multi-line scanning with selected pulse overlap rate was performed, and large-area micro-cracks being similar to the dry-land in nature were formed under very low laser power intensity. Surface characteristics of the irradiated regions were further characterized by X-ray diffraction (XRD) and energy dispersive X-ray spectroscopy (EDS), and accordingly, the formation mechanism of micro-cracks was discussed. These results would not only be helpful to understand some microstructures observed under the relatively high laser power intensity, but also be meaningful to guide the selection of laser parameters for various applications.

2. Materials and experiments

As-cast rod-shaped $Zr_{41.2}Ti_{13.8}Cu_{12.5}Ni_{10}Be_{22.5}$ MG (commonly called Vitreloy 1) with a diameter of 10 mm was cut into pieces with thickness of 2 mm by wire-electrical discharge machining (Wire-EDM). To remove the EDM-induced surface crystallization layer [28,29], these pieces were ground by using 400, 800, and 1500 grit sand papers in sequence, followed by polishing using diamond abrasive paste and cleaning with acetone.

A Nd:YAG nanosecond pulsed laser system (LR-SHG, MegaOpto Co., Ltd., Japan) with a wavelength of 532 nm and pulse width of 15.4 ns was used to irradiate the MG sample. The laser beam with a Gaussian energy distribution was focused to a spot with diameter of 85 μm by the F-theta lens. During laser irradiation, a constant pulse frequency of 1 kHz was employed, and the average laser powers were varied from 0.02 to 0.06 W, corresponding to the peak laser power intensities varying from 2.3×10^{11} to 6.9×10^{11} W/m^2 (being an order of magnitude lower than the commonly used one). Three kinds of scanning speeds, 1, 5, and 10 mm/s corresponding to 1000, 200, and 100 pulses per 1 mm, were used to investigate the effects of laser scanning speed on the surface characteristics of the irradiated regions. Both single-line scanning and multi-line scanning were implemented. During multi-line scanning, the distances between two adjacent scanning lines were selected to be 43 and 85 μm, corresponding to the pulse overlap rates of 50% and 0%, respectively.

To comprehensively observe the surface characteristics after laser irradiation, both the scanning electron microscope (Inspect S50 and F50, FEI, USA) and white light interferometer (Talysurf CCI1000, AMETEX Taylorhobson Ltd., UK) were employed. For SEM observation using Inspect S50, the acceleration voltage, spot size, and working distance (WD) were 5.00 kV, 3.0, and 10.2 mm, respectively; when using Inspect F50, they were 10.00 kV, 3.0, and 11.1 mm, respectively.

The element distribution in the laser irradiated regions was measured by the energy dispersive X-ray spectroscopy (EDS, XFlash Detector 4010, Bruker, Germany), which was integrated with Inspect F50. During EDS measurement, the employed acceleration voltage and live time were 15 kV and 93 s, respectively. In addition, an X-ray diffractometer (XRD, D8 Discover, Bruker, Germany) was used to verify whether the amorphous characteristic had been changed before and after laser irradiation. The multi-line laser scanned regions obtained under two different pulse overlap rates as well as the originally polished surface were characterized. The voltage and current of the X-ray generator were 40 kV and 40 mA, respectively. The 2θ angle was scanned from 12.40° to 107.60° with the sampling interval of 0.01°, and the total scanning time was about 180 s.

3. Results and discussion

3.1. Surface microstructures

Figs. 1 (a) to (d) show the SEM morphologies of the single-line

irradiated region with different magnifications and positions. The employed peak laser power intensity and scanning speed are 2.3×10^{11} W/m^2 and 1 mm/s, respectively. From the overall morphology as shown in Fig. 1(a), it is seen that many interlaced micro-cracks are generated in the irradiated region. Furthermore, these micro-cracks propagate along the laser scanning direction as shown in Fig. 1(b) where the morphology around the center of the scanning line is presented. Fig. 1(d) is a local enlarged view of Fig. 1(b), and two kinds of micro-cracks are clearly observed, the relatively wide one and the relatively narrow one. The wider one is named as the primary crack and its maximum width is about 3 μm; the other one is named as the secondary crack. The secondary cracks are distributed on both sides of the primary cracks. Fig. 1(c) shows the morphology around the end of the scanning line, and these two kinds of micro-cracks also appear. Fig. 1(e) presents the three-dimensional (3D) topography of the irradiated region, and Fig. 1(f) shows the profile along the marked line in Fig. 1(e). It is seen that the depth of the primary crack is over 200 nm. Furthermore, almost the entire irradiated region is slightly higher than the initially polished surface. The above results indicate that micro-cracks with depth in nanoscale and width in microscale have been generated under the current experimental parameters.

Generally, for single-line scanning, the resultant surface microstructures are mainly related to the scanning speed and peak laser power intensity. Therefore, the effects of these two parameters are further investigated. Fig. 2 presents the results obtained under two increased scanning speeds, 5 and 10 mm/s. For comparison with the results in Fig. 1, the same peak laser power intensity of 2.3×10^{11} W/m^2 is employed during experiments. As shown in Figs. 2(a) to (c), when increasing the scanning speed to 5 mm/s, the primary cracks become significantly narrower than those obtained under 1 mm/s, and its maximum width is less than 1 μm; furthermore, the secondary cracks disappear. When further increasing the scanning speed to 10 mm/s, both the primary crack and the secondary crack are not observed, and only the surface scratches generated during polishing are enhanced due to their enhanced absorption of laser energy compared to the surrounding non-scratch regions. Via white light interferometer, the depth of the primary-crack generated under 5 mm/s is measured to be about 40 nm which is much less than that obtained under 1 mm/s. The comparative results in Figs. 1 and 2 indicate that under the same peak laser power intensity of 2.3×10^{11} W/m^2, when increasing the scanning speed from 1 to 10 mm/s, the micro-cracks become narrower and shallower, and finally disappear.

Fig. 3 presents the SEM morphologies of single-line irradiated regions when increasing the peak laser power intensity to 4.6×10^{11} W/m^2 (Figs. 3(a)–(c)) and 6.9×10^{11} W/m^2 (Figs. 3(d)-(f)). The scanning speed is kept to be 1 mm/s. In Figs. 3(a)-(c), the laser pulse tracks and open cracks are clearly observed, and furthermore, some line cracks appear around the center of the scanning line. It is easy to find that these line cracks are originated from those open cracks generated on both sides of the scanning line. When further increasing the peak laser power intensity to 6.9×10^{11} W/m^2, although the open cracks are still clearly visible on both sides of the scanning line, line cracks have been significantly weakened around the center when comparing Figs. 3(e) with 3(b). However, near the two sides of the scanning line, line cracks are still clearly observed. Figs. 4(a) and (c) show the 3D topographies of the regions irradiated under the peak laser power intensities of 4.6×10^{11} W/m^2 and 6.9×10^{11} W/m^2, respectively, and Figs. 4(b) and (d) show the profiles along the marked lines in Figs. 4(a) and (c), respectively. The typical micro-groove structure is formed on the MG surface, instead of the micro-cracks as shown in Fig. 1. In Fig. 4(b), the height of pileup is about 130 nm and the depth of micro-groove is about 100 nm. In Fig. 4(d), when increasing the peak laser power intensity to 6.9×10^{11} W/m^2, the height of pileup increases to be about 160 nm and the depth of micro-groove increases to be about 260 nm. This is easy to understand that increasing the peak laser power intensity, the recoil pressure and the molten/vaporized materials will increase, resulting in
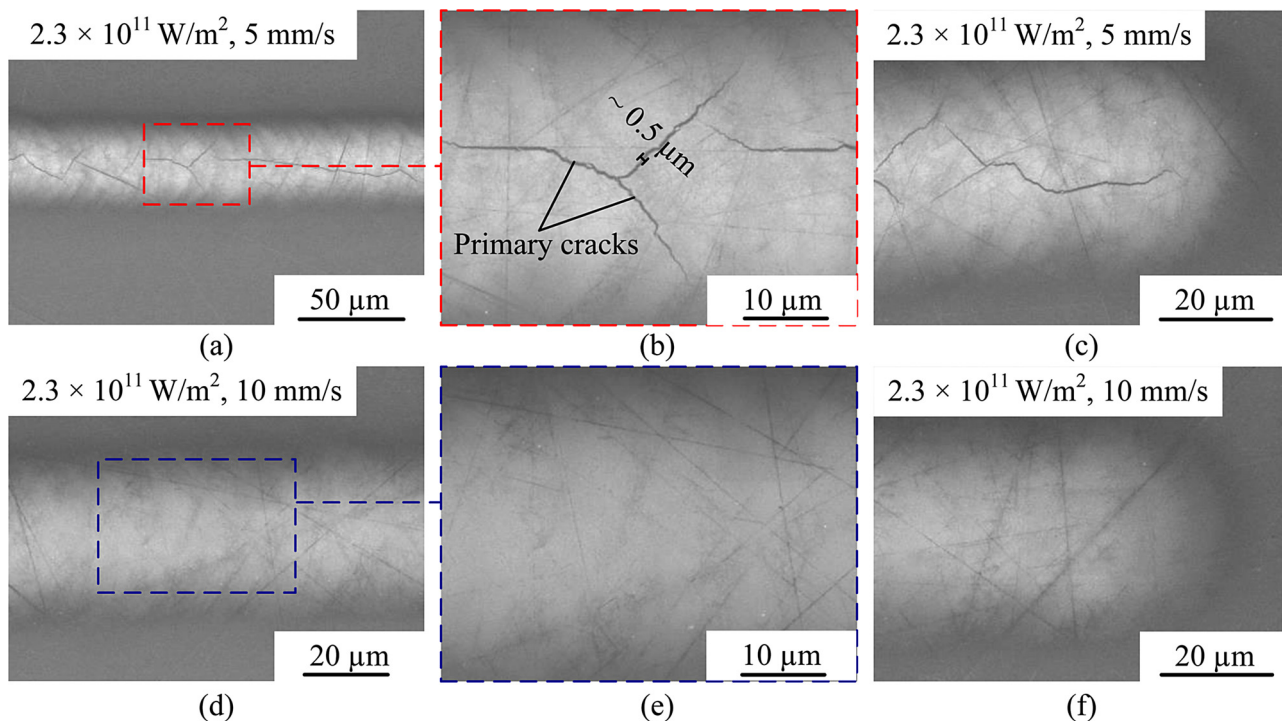
Fig. 2. (a)-(f) SEM morphologies obtained by increasing the scanning speed to 5 mm/s ((a)-(c)) and 10 mm/s ((d)-(f)). The peak laser power intensity is kept to be the same with that of Fig. 1 (2.3×10^{11} W/m^2).

the increase in height of pileup and depth of micro-groove. According to Figs. 3 and 4, when increasing the peak laser power intensity, the micro-groove structure would be formed with some line cracks, open cracks and laser pulse tracks on it.

From the above results obtained by single-line laser scanning, it is known that under the peak laser power intensities of 4.6×10^{11} W/m^2 and 6.9×10^{11} W/m^2, the micro-groove structure with pileup around it

and cracks on it is generated on the irradiated region; when decreasing the peak laser power intensity to 2.3×10^{11} W/m^2, micro-cracks are formed on the laser scanned line. Next, multi-line laser scanning was performed to investigate the evolution of surface characteristics. As an example, Fig. 5 presents the SEM morphologies of multi-line laser scanned surfaces under the relatively low peak laser power intensity of 2.3×10^{11} W/m^2 and different pulse overlap rates r, 50% (Figs. 5(a)
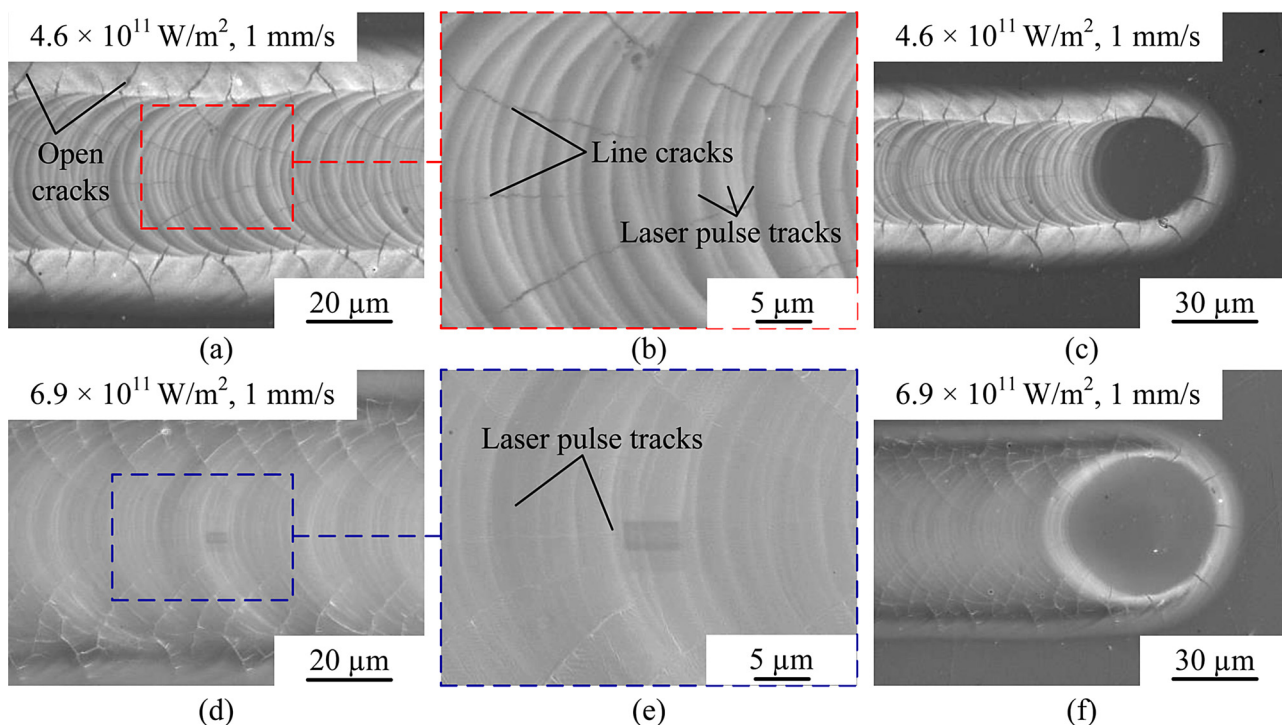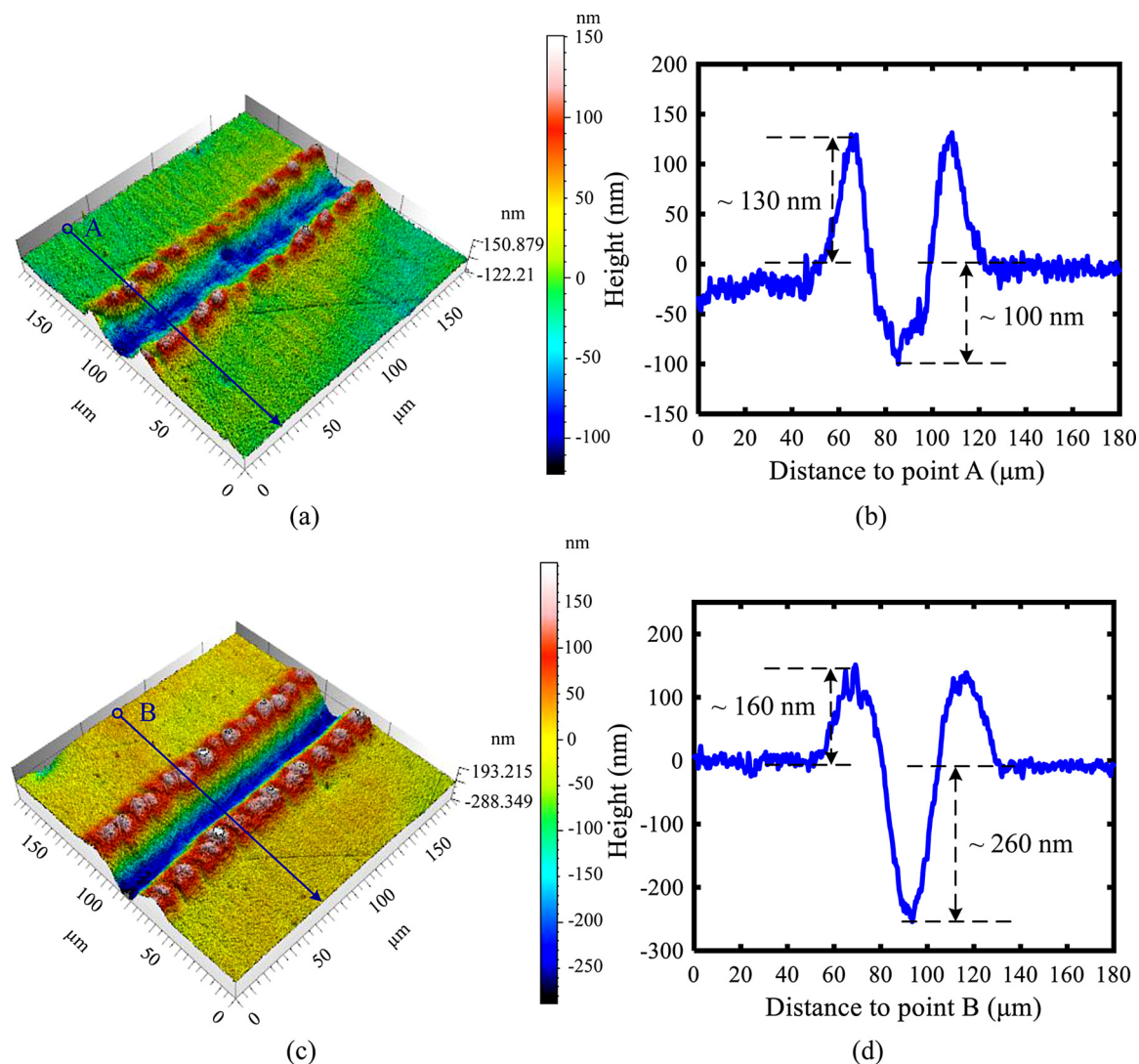

Fig. 3. SEM morphologies obtained by increasing the peak laser power intensity to 4.6×10^{11} W/m^2 ((a)-(c)) and 6.9×10^{11} W/m^2 ((d)-(f)). The scanning speed is kept to be the same with that in Fig. 1 (1 mm/s).

Fig. 4. 3D topographies of the regions irradiated under different peak laser power intensities: (a) 4.6×10^{11} W/m^2 and (c) 6.9×10^{11} W/m^2. (b) and (d) show the profiles of the marked lines in Figs. 4(a) and (c), respectively.

and (b)) and 0% (Figs. 5(c) and (d)). Other experimental parameters are inserted in the figure. In Fig. 5(a), micro-cracks are distributed on the entire irradiated regions, and in Fig. 5(b), it is seen that some primary cracks generated around the center of two adjacent scanning lines have connected to each other. According to the corresponding 3D topography as shown in Fig. 6(a), the entire irradiated region is very like a dry-land in nature. As shown in Fig. 5(c), when reducing the pulse overlap rate from 50 % to 0%, the primary cracks still exist around the center of each scanning line, but they are no longer connected to each other. Instead, they are separated by the narrow interaction area on both sides of the scanning line. From the corresponding 3D topography as shown in Fig. 6(b), some micro-cracks with larger length could be observed. The comparative results in Fig. 5 and indicate that the pulse overlap rate also significantly affects the formation and distribution of micro-cracks during multi-line laser scanning of MG.

Fig. 7 shows SEM morphologies of multi-line laser scanned surfaces under an increased peak laser power intensity of 6.9×10^{11} W/m^2 and different pulse overlap rates r, 50% (Figs. 7(a) and (b)) and 0% (Figs. 7(c) and (d)). Other experimental parameters are inserted in the figure. Fig. 8 presents the corresponding 3D topographies. In Fig. 8, regardless of the pulse overlap rate being 50% or 0%, the irradiated surface is like a piece of farmland with the pileup as the ridge and the micro-groove as furrow. In addition, compared to Fig. 8(b), when

increasing the pulse overlap rate from 0% to 50%, the pileup formed in the preceding scanning line could be effectively combined, making it more regular as shown in Fig. 8(a).

3.2. Surface characteristics measured by XRD and EDS

As the formation of micro-groove structure has been widely reported and investigated previously, the following emphasis will be on the formation mechanism of micro-cracks induced by nanosecond pulsed laser irradiation. Accordingly, the irradiated regions are further characterized by XRD and EDS. Fig. 9 presents the XRD patterns measured on the multi-line laser irradiated regions as well as the originally polished surface. All the XRD patterns display only one broad hump and no other sharp crystal peaks, demonstrating that under various laser parameters, the irradiated regions maintain the amorphous characteristic. This is due to the fast heating and cooling rates during nanosecond pulsed laser irradiation. The results in Fig. 9 indicate that these microcracks in the laser irradiated regions are not caused by the crystallization of MG.

In Figs. 1(b) to (d), the contrast and brightness between the inside and outside of the micro-crack are significantly different, which may suggest the difference in composition. Therefore, by using EDS, the elements inside and outside of the micro-cracks are measured.
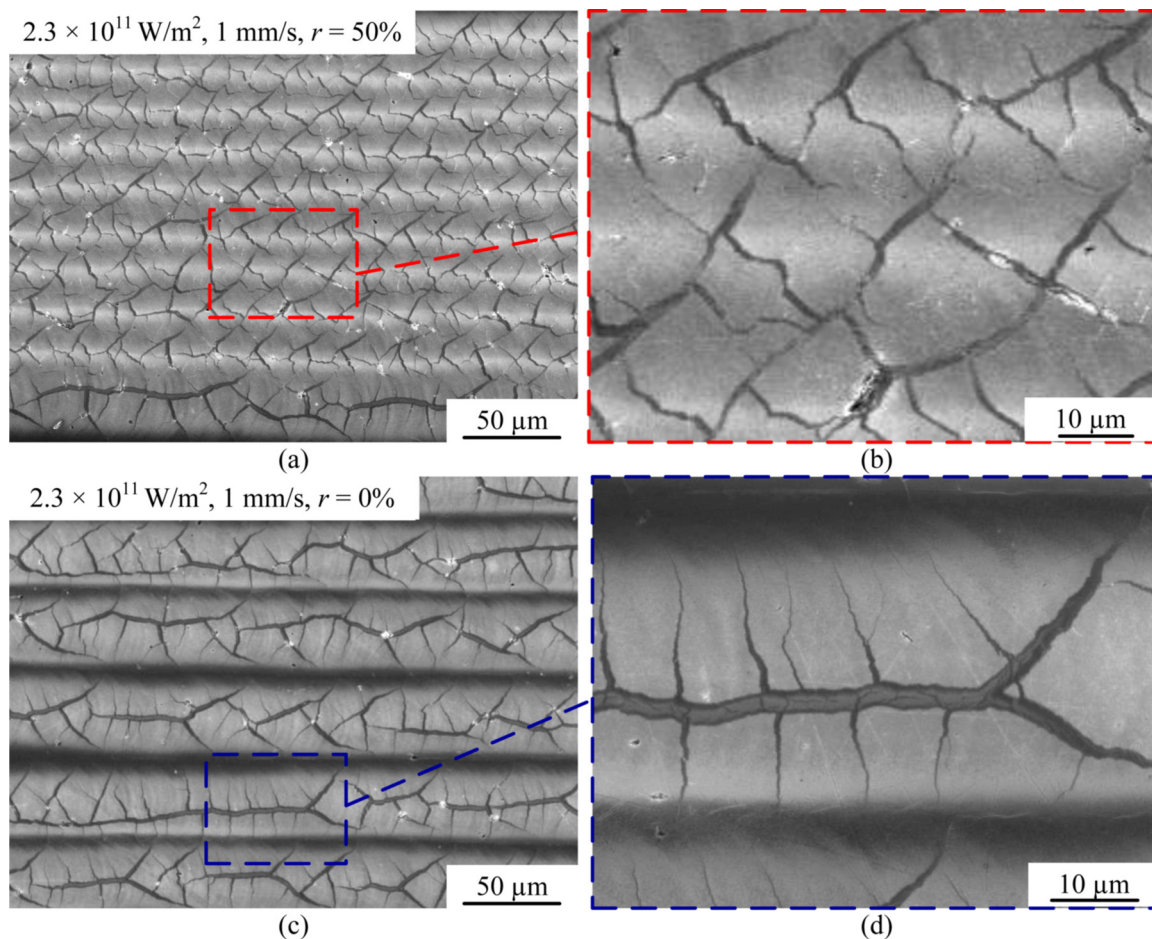
Fig. 5. SEM morphologies of multi-line laser scanned regions under the relatively low peak laser power intensity of 2.3×10^{11} W/m^2 and different pulse overlap rates: (a) and (b) $r = 50\%$, (c) and (d) $r = 0\%$. Other experimental parameters are inserted in the figure.
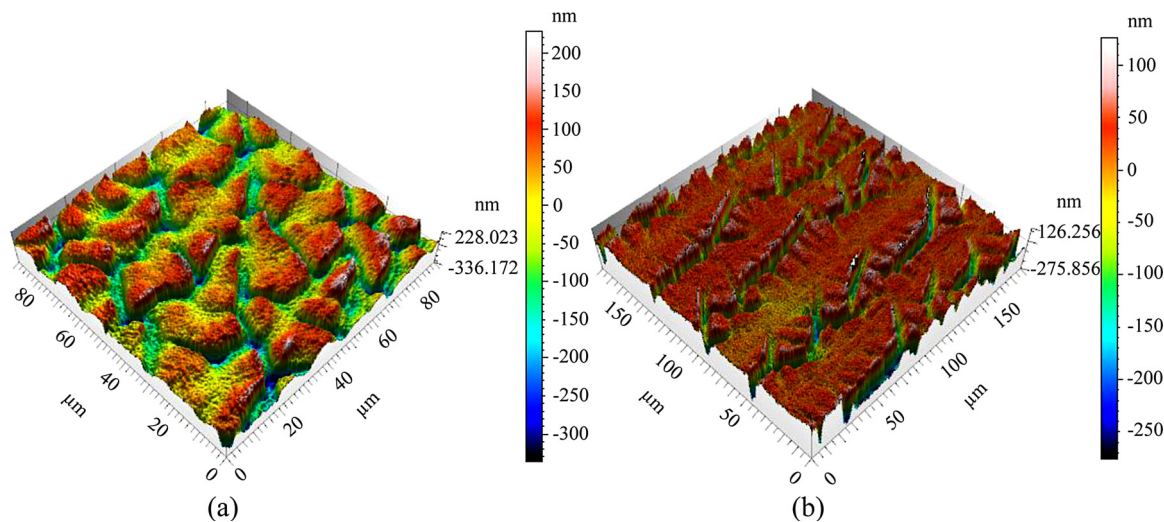

Fig. 6. 3D topographies of multi-line laser scanned regions under the relatively low peak laser power intensity of 2.3×10^{11} W/m^2 and different pulse overlap rates: (a) $r = 50\%$ and (b) $r = 0\%$. Other experimental parameters are the same to those in Fig. 5.

Figs. 10(a) and (b) show the positions for single spot measurement, one inside the micro-crack and another outside the micro-crack. The statistic results of the element content are listed in Table 1. Although the MG sample contains Be element, it is difficult to be detected by EDS because it is a light chemical element. The statistical results listed in Table 1 indicate that the element content inside and outside of the micro-crack is not changed. The above results demonstrate that the employed laser parameters do not lead to element enrichment, and it is not the reason for the formation of micro-cracks.
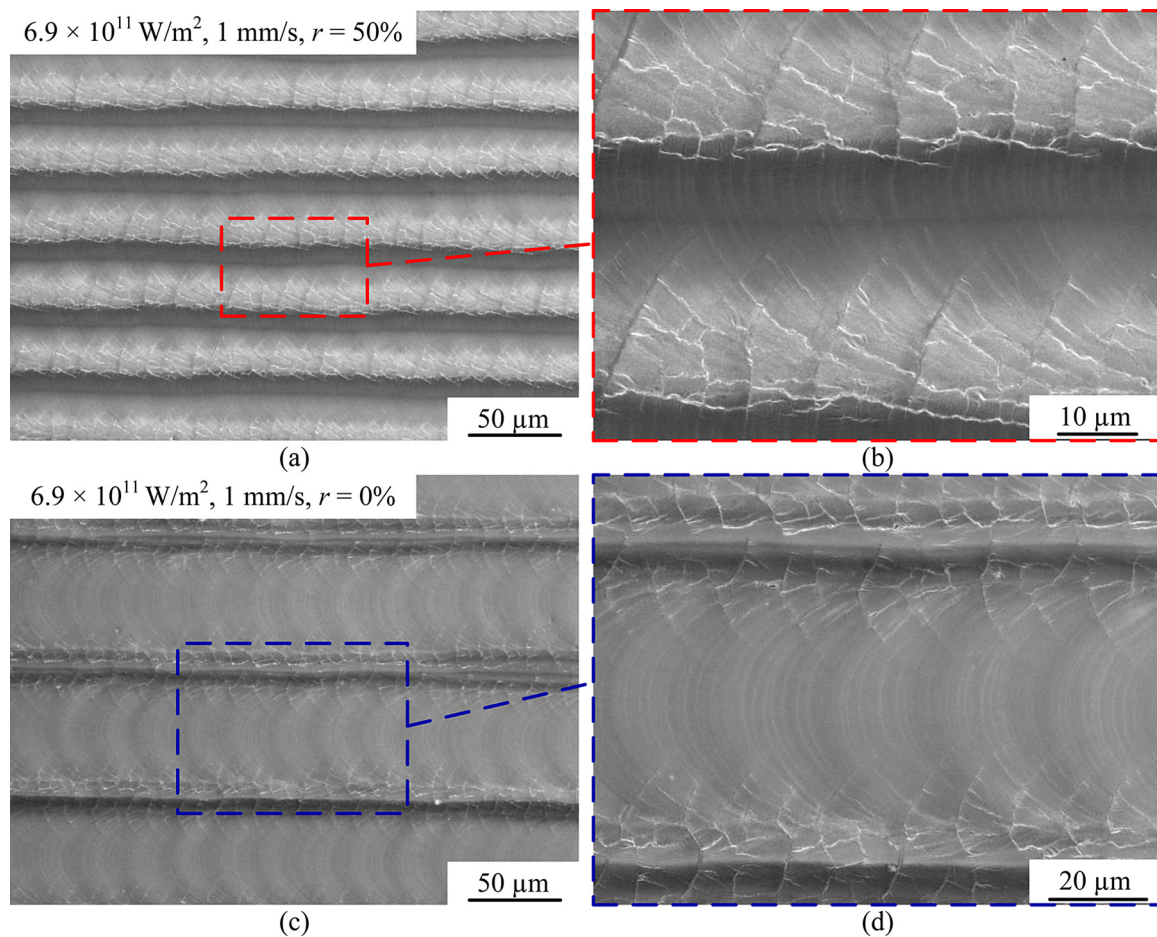
Fig. 7. SEM morphologies of multi-line laser scanned regions under an increased peak laser power intensity of 6.9×10^{11} W/m^2 and different pulse overlap rates: (a) and (b) $r = 50\%$, (c) and (d) $r = 0\%$. Other experimental parameters are inserted in the figure.

3.3. Formation mechanism of the micro-cracks

The XRD and EDS results indicate that under the current experimental parameters, no crystallization and element enrichment occur during nanosecond pulsed laser irradiation. Therefore, the micro-cracks may be caused by some other reasons. By further analyzing the morphology and distribution of micro-cracks as well as the irradiation

process, the formation of micro-cracks could be mainly due to the tensile stress generated during the re-solidification process. Taking the single-line scanning of MG as an example, Fig. 11 shows a schematic diagram, illustrating the formation mechanism of micro-cracks. When the nanosecond pulsed laser irradiates the MG surface, the MG absorbs a portion of laser energy in a very short time and further diffuses internally in the form of heat [20,26]. At the same time, the high
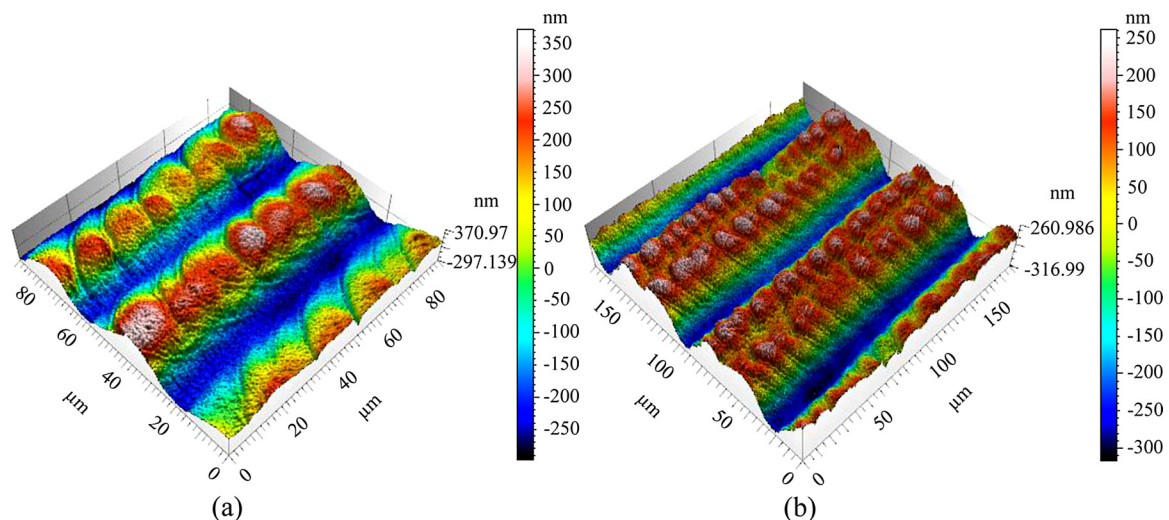

Fig. 8. 3D topographies of multi-line laser scanned regions under an increased peak laser power intensity of 6.9×10^{11} W/m^2 and different pulse overlap rates: (a) $r = 50\%$ and (b) $r = 0\%$. Other experimental parameters are the same to those in Fig. 7.
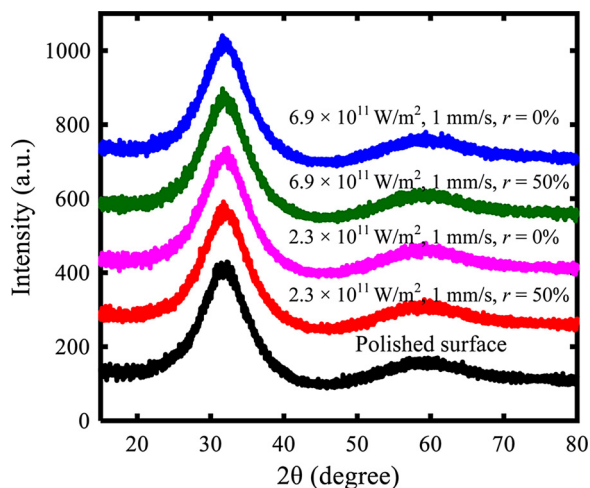
Fig. 9. XRD patterns of the multi-line laser irradiated regions as well as the originally polished MG surface. Detailed experimental parameters are inserted in the figure.

Table 1
Atomic percent of each element obtained for Spot 1 and Spot 2 (at. %).

Element	Zr	Ti	Ni	Cu
Spot 1	49.22	19.24	13.30	18.23
Spot 2	49.34	19.25	13.30	18.11

Fig. 11. Schematic diagrams illustrating the formation mechanism of primary crack and secondary crack in the single-line laser irradiated region.

temperature generated by laser irradiation would create a molten pool on the MG surface. When the peak laser power intensity is very low such as 2.3×10^{11} W/m^2 in this study, the molten pool would be quite thin, which would not significantly damage the originally polished surface. Since the thermal conductivity of Zr-based MG is relatively low, a high temperature gradient will be generated on both sides of the laser scanning line, and the direction of temperature gradient will be perpendicular to the laser scanning direction [30]. When the laser pulse has passed, rapid cooling and re-solidification will occur. As the temperature of non-irradiated regions is much lower than that of the irradiated regions, re-solidification will start from the non-irradiated region to the irradiated region, and two sides of the laser scanning line will progress simultaneously. With the re-solidification, MG materials will shrink, and finally around the center of the scanning line, a relatively high tensile stress would appear. As the tensile plasticity of Vitreloy 1 is quite poor [31–35], when the tensile stress exceeds a certain value, the micro-crack would be formed. Once one primary crack has been generated, the local stress is greatly released. Therefore, the generation of next primary crack requires further stress accumulation, and this may be the reason why the primary cracks in Figs. 1 and 5 are intermittent. As shown in Figs. 1 and 10, the edges of primary cracks are relatively rough, and they provide the potential nucleation sites for generation of secondary cracks. With the role of local stress, secondary cracks would originate from the edges of primary cracks.

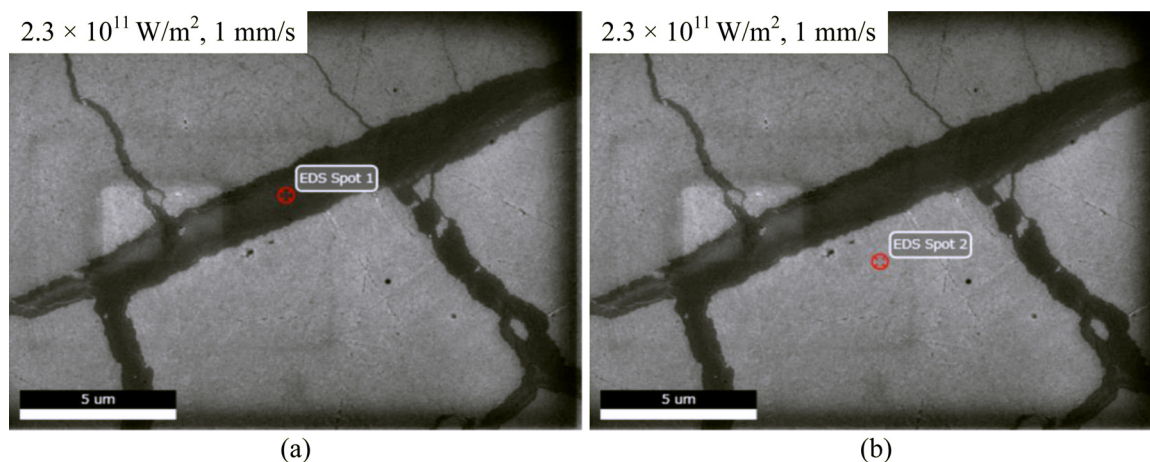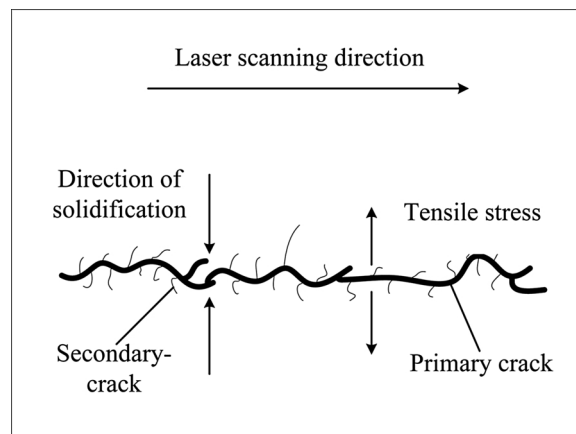With regards to the effects of laser scanning speed, when increasing the scanning speed from 1 mm/s to 5 mm/s, the number of laser pulses per unit length is decreased, and thus the heat accumulation resulting from the preceding laser pulses is weakened. Accordingly, the molten MG materials under 5 mm/s would be significantly less than that under 1 mm/s. This could be further confirmed by the following fact: in Figs. 2(b) and (c), the surface scratches generated during the polishing process are still visible, but they are almost not visible in Figs. 1(b) and (c). Therefore, the tensile stress around the center of the laser scanning line under 5 mm/s is much lower than that under 1 mm/s, resulting in the narrowed micro-cracks. Further increasing the scanning speed to 10 mm/s, no micro-cracks appear as shown in Figs. 2(d) to (f) because the induced stress is too low, being not over the critical value for generation of visible micro-crack.

With regards to the effects of peak laser power intensity, when increasing the peak laser power intensity, the molten MG materials will increase. With the role of recoil pressure, some MG materials will flow toward the sides of the laser scanning line, and thus the micro-groove with pileup around it will be formed [16,36]. The formation of open cracks as well as line cracks actually is also due to the tensile stress generated during the re-solidification process. When increasing the

Fig. 10. The positions for single spot EDS measurement: (a) inside the micro-crack and (b) outside the micro-crack.

peak laser power intensity from 4.6×10^{11} W/m^2 to 6.9×10^{11} W/m^2, the reduced line cracks around the center of the laser scanning line may be mainly due to the healing role of subsequent laser pulse under a relatively high peak laser power intensity. This could be reasonable because cracks have enhanced absorption of laser energy compared with these regions free of cracks. During the subsequent laser pulse irradiation, localized material flow would occur around the previously formed line cracks because of their enhanced absorption of laser energy, leading to the healing of line cracks. This could be also verified by analyzing the cracks formed around the last laser pulse point. For a single pulse point, open cracks with similar size could be uniformly distributed around it. However, as shown in Figs. 3(c) and (f), the cracks on the left side are obviously weakened compared with the cracks on the right side, further confirming the healing role of subsequent laser pulse.

4. Conclusions

In summary, surface microstructures and characteristics of a polished Zr-based MG after nanosecond pulsed laser irradiation under relatively low peak laser power intensities were investigated in detail. By experiments and analysis, the following conclusions could be derived.

The micro-cracks with depth in nanoscale and width in microscale were generated on the Zr-based MG surface under a very low peak laser power intensity (2.3×10^{11} W/m^2).

Under the peak laser power intensity of 2.3×10^{11} W/m^2, when increasing the scanning speed from 1 mm/s to 5 mm/s, the micro-cracks became narrower and shallower; further increasing the scanning speed to 10 mm/s, no micro-cracks appeared, and the surface scratches generated during polishing were clearly visible.

Under the scanning speed of 1 mm/s, increasing the peak laser power intensity from 2.3×10^{11} W/m^2 to 4.6×10^{11} W/m^2, the micro-groove structure was generated on the MG surface. Furthermore, around the micro-groove, there were pileup and open cracks; on the surface of micro-groove, there were some line cracks and laser pulse tracks.

During multi-line laser scanning, the laser irradiation parameters significantly affected the formation and distribution of micro-cracks. Under selected parameters, the multi-line laser scanned surface was similar to the dry-land in nature.

The XRD and EDS results indicated that under the current experimental parameters, no crystallization and element enrichment occurred during nanosecond pulsed laser irradiation. By analyzing the morphology and distribution of micro-cracks as well as the irradiation process, the formation of micro-cracks could be mainly due to the tensile stress generated during the re-solidification process.

According to this study, when performing laser polishing of MGs, the processing parameters such as the peak laser power intensity and the scanning speed should be carefully optimized to avoid the generation of micro-cracks as well as the micro-groove that may deteriorate the surface quality.

Declaration of Competing Interest

The authors declare that they have no known competing financial interests or personal relationships that could have appeared to influence the work reported in this paper.

Acknowledgements

References

[1] M.M. Trexler, N.N. Thadhani, Mechanical properties of bulk metallic glasses, Prog. Mater. Sci. 55 (2010) 759–839.

[2] A. Inoue, Bulk glassy alloys: historical development and current research, Engineering 1 (2015) 185–191.

[3] A. Inoue, A. Takeuchi, Recent development and application products of bulk glassy alloys, Acta Mater. 59 (2011) 2243–2267.

[4] J. Plummer, W.L. Johnson, Is metallic glass poised to come of age? Nat. Mater. 14 (2015) 553–555.

[5] M. Telford, The case for bulk metallic glass, Mater. Today 7 (2004) 36–43.

[6] E. Williams, N. Lavery, Laser processing of bulk metallic glass: a review, J. Mater. Process. Technol. 247 (2017) 73–91.

[7] Y.Y. Shen, Y.Q. Li, C. Chen, H.L. Tsai, 3D printing of large, complex metallic glass structures, Mater. Des. 117 (2017) 213–222.

[8] Y.Q. Li, Y.Y. Shen, M.C. Leu, H.L. Tsai, Building Zr-based metallic glass part on Ti-6Al-4V substrate by laser foil-printing additive manufacturing, Acta Mater. 144 (2018) 810–821.

[9] B. Chen, T.L. Shi, M. Li, F. Yang, F. Yan, G.L. Liao, Laser welding of annealed Zr$_{55}$Cu$_{30}$Ni$_5$Al$_{10}$ bulk metallic glass, Intermetallics 46 (2014) 111–117.

[10] G. Wang, Y.J. Huang, M. Shagiev, J. Shen, Laser welding of Ti$_{40}$Zr$_{25}$Ni$_3$Cu$_{12}$Be$_{20}$ bulk metallic glass, Mater. Sci. Eng. A 541 (2012) 33–37.

[11] D. Ouyang, W. Xing, N. Li, Y.C. Li, L. Liu, Structural evolutions in 3D-printed Fe-based metallic glass fabricated by selective laser melting, Addit. Manuf. 23 (2018) 246–252.

[12] J. Fu, Y.H. Zhu, C. Zheng, R. Liu, Z. Ji, Effect of laser shock peening on the compressive deformation and plastic behavior of Zr-based bulk metallic glass, Opt. Lasers Eng. 86 (2016) 53–61.

[13] Y.S. Li, K. Zhang, Y. Wang, W.Q. Tang, Y.T. Zhang, B.C. Wei, Z. Hu, Abnormal softening of Ti-metallic glasses during nanosecond laser shock peening, Mater. Sci. Eng. A 773 (2020) 138844.

[14] M. Liang, Y.H. Zhu, Z. Li, J. Fu, C. Zheng, Effect of laser shock peening and its size-dependence on the compressive plasticity of Zr-based bulk metallic glass, J. Mater. Process. Technol. 251 (2018) 47–53.

[15] L. Wang, L. Wang, Z.H. Nie, Y. Ren, Y.F. Xue, R.H. Zhu, H.F. Zhang, H.M. Fu, Evolution of residual stress, free volume, and hardness in the laser shock peened Ti-based metallic glass, Mater. Des. 111 (2016) 473–481.

[16] H. Huang, J.W. Yan, Surface patterning of Zr-based metallic glass by laser irradiation induced selective thermoplastic extrusion in nitrogen gas, J. Micromech. Microeng. 27 (2017) 075007.

[17] H. Huang, N. Jun, M.Q. Jiang, M. Ryoko, J.W. Yan, Nanosecond pulsed laser irradiation induced hierarchical micro/nanostructures on Zr-based metallic glass substrate, Mater. Des. 109 (2016) 153–161.

[18] L. Zhang, H. Huang, Micro machining of bulk metallic glasses: a review, Int. J. Adv. Manuf. Technol. 100 (2019) 637–661.

[19] Y. Jiao, E. Brousseau, Q.Q. Han, H.X. Zhu, S. Bigot, Investigations in nanosecond laser micromachining on the Zr$_{52.8}$Cu$_{17.6}$Ni$_{14.8}$Al$_{9.9}$Ti$_{4.9}$ bulk metallic glass: experimental and theoretical study, J. Mater. Process. Technol. 273 (2019) 116232.

[20] E. Williams, E.B. Brousseau, Nanosecond laser processing of Zr$_{41.2}$Ti$_{13.8}$Cu$_{12.5}$Ni$_{10}$Be$_{22.5}$ with single pulses, J. Mater. Process. Technol. 232 (2016) 34–42.

[21] Y. Jiao, E. Brousseau, X.J. Shen, X.X. Wang, Q.Q. Han, H.X. Zhu, S. Bigot, W.F. He, Investigations in the fabrication of surface patterns for wettability modification on a Zr-based bulk metallic glass by nanosecond laser surface texturing, J. Mater. Process. Technol. 283 (2020) 116714.

[22] M.Q. Jiang, X.Q. Wu, Y.P. Wei, G. Wilde, L.H. Dai, Cavitation bubble dynamics during pulsed laser ablation of a metallic glass in water, Extreme Mech. Lett. 11 (2017) 24–29.

[23] J. Fu, Y.H. Zhu, C. Zheng, R. Liu, Z. Ji, Effect of laser shock peening on mechanical properties of Zr-based bulk metallic glass, Appl. Surf. Sci. 313 (2014) 692–697.

[24] Y. Liu, M.Q. Jiang, G.W. Yang, Y.J. Guan, L.H. Dai, Surface rippling on bulk metallic glass under nanosecond pulse laser ablation, Appl. Phys. Lett. 99 (2011) 191902.

[25] Y. Liu, M.Q. Jiang, G.W. Yang, J.H. Chen, Y.J. Guan, L.H. Dai, Saffman–Taylor fingering in nanosecond pulse laser ablating bulk metallic glass in water, Intermetallics 31 (2012) 325–329.

[26] M.Q. Jiang, Y.P. Wei, G. Wilde, L.H. Dai, Explosive boiling of a metallic glass superheated by nanosecond pulse laser ablation, Appl. Phys. Lett. 106 (2015) 021904.

[27] H. Huang, M.Q. Jiang, J.W. Yan, The coupling effects of laser thermal shock and surface nitridation on mechanical properties of Zr-based metallic glass, J. Alloys. Compd. 770 (2019) 864–874.

[28] H. Huang, J.W. Yan, On the surface characteristics of a Zr-based bulk metallic glass processed by microelectrical discharge machining, Appl. Surf. Sci. 355 (2015) 1306–1315.

[29] H. Huang, J.W. Yan, Microstructural changes of Zr-based metallic glass during microelectrical discharge machining and grinding by a sintered diamond tool, J. Alloys. Compd. 688 (2016) 14–21.

[30] D. Ouyang, N. Li, W. Xing, J.J. Zhang, L. Liu, 3D printing of crack-free high strength Zr-based bulk metallic glass composite by selective laser melting, Intermetallics 90 (2017) 128–134.

[31] L. Zhang, F. Jiang, D. Zhang, L. He, J. Sun, J. Fan, Z. Zhang, In-Situ Precipitated nanocrystal Beneficial to Enhanced Plasticity of Cu-Zr Based bulk Metallic Glasses,

Adv. Eng. Mater. 10 (2008) 943–950.

[32] G. Chen, H. Bei, Y. Cao, A. Gali, C.T. Liu, E.P. George, Enhanced plasticity in a Zr-based bulk metallic glass composite with in situ formed intermetallic phases, Appl. Phys. Lett. 95 (2009) 081908.

[33] J.W. Qiao, Y. Zhang, G.L. Chen, Fabrication and mechanical characterization of a series of plastic Zr-based bulk metallic glass matrix composites, Mater. Des. 30 (2009) 3966–3971.

[34] M.J. Xu, J.J. Xu, H. Lu, J.S. Chen, J.M. Chen, X. Wei, Fractal and probability analysis of creep crack growth behavior in 2.25Cr–1.6W steel incorporating residual stresses, Appl. Surf. Sci. 359 (2015) 73–81.

[35] M.M. Alam, Z. Barsoum, P. Jonsén, A.F.H. Kaplan, H.Å. Häggblad, The influence of surface geometry and topography on the fatigue cracking behaviour of laser hybrid welded eccentric fillet joints, Appl. Surf. Sci. 256 (2010) 1936–1945.

[36] V. Semak, A. Matsunawa, The role of recoil pressure in energy balance during laser materials processing, J. Phys. D Appl. Phys. 30 (1997) 2541–2552.